The Astrophysical Journal, 703:930–938, 2009 September 20 doi:10.1088/0004-637X/703/1/930

HUBBLE SPACE TELESCOPE IMAGES AND KPNO SPECTROSCOPY OF THE BINARY BLACK HOLE CANDIDATE SDSS J153636.22+044127.0*

Tod R. Lauer and Todd A. Boroson
National Optical Astronomy Observatory, P.O. Box 26732, Tucson, AZ 85726, USA
Received 2009 May 28; accepted 2009 August 5; published 2009 September 2

ABSTRACT

We present *Hubble Space Telescope* WFPC2/PC images and KPNO 4 m long-slit spectroscopy of the QSO SDSS J153636.22+044127.0, which we advanced as a candidate binary supermassive black hole. The images reveal a close companion coincident with the radio source identified by Wrobel & Laor. It appears to be consistent with a $M_g \sim -21.4$ elliptical galaxy, if it is at the QSO redshift. The spectroscopy, however, shows no spatial offset between the red or blue Balmer lines. The companion is thus not the source of either the red or blue broad-line systems; SDSS J153636.22+044127.0 is highly unlikely to be a chance superposition of objects or an ejected black hole. Over the $\Delta T = 0.75$ yr difference between the rest-frame epoch of the present and SDSS spectroscopy, we find no velocity shift to within 40 km s^{-1}, nor any amplitude change in either broad-line system. The lack of a shift can be admitted under the binary hypothesis, if the implied radial velocity is a larger component of the full orbital velocity than was assumed in our earlier work. A strong test of the binary hypothesis requires yet longer temporal baselines. The lack of amplitude variations is unusual for the alternative explanation of this object as a "double-peaked" emitter; we further argue that SDSS J153636.22+044127.0 has unique spectral features that have no obvious analogue with other members of this class.

Key words: black hole physics – quasars: emission lines – quasars: individual (SDSS J153636.22+044127.0)

Online-only material: color figures

1. A BINARY SUPERMASSIVE BLACK HOLE CANDIDATE

The low-redshift QSO SDSS J153636.22+044127.0 (hereafter J1536+0441) is a candidate for hosting a binary supermassive black hole (Boroson & Lauer 2009). Its spectrum exhibits two broad-line emission systems at $z = 0.388$ and $z = 0.373$, thus separated in velocity by 3500 km s^{-1}, but only one narrow-line system, which is associated with the redder or "*r*" broad-line system. A third system of unresolved absorption lines has an intermediate velocity. These characteristics are unique among known quasars. We advanced this object as a candidate binary system of two supermassive black holes. The rough estimates of the two black hole masses are $10^{8.9}\ M_\odot$ and $10^{7.3}\ M_\odot$, based on line and continuum properties. Under this picture, the velocity difference between the broad-line systems is the projected orbital velocity difference of the two black holes. Assuming a circular orbit with random phase and inclination, we derive the separation of the black holes and their orbital period to be ~ 0.1 parsec and ~ 100 years, respectively.

There is strong interest in the prevalence of binary black hole systems, which should be commonly formed in the formation of galaxies from hierarchical merging of smaller systems (Volonteri et al. 2003). This has motivated several observational searches for binary systems; however, few compelling candidates have survived scrutiny. Likewise, other investigators have quickly attempted to obtain additional observations of J1536+0441 to ascertain its viability as a binary system. These works, rather than confirming the binary hypothesis, have offered other interpretations.

Chornock et al. (2009) obtained a spectrum of J1536+0441 that covered longer wavelengths than those that were sampled by the SDSS spectrum. They identified a "bump" in the red-wing of the *r*-system Hα line that has a corresponding weak feature in the Mg II λ2800 line. At Hβ, the presence of this red bump is ambiguous due to its near overlap with the 4959 Å [O III] line. Further, the red bump and *b*-system (bluer) Balmer lines are roughly symmetrical about the *r*-system lines. The red bump, and in particular its apparent symmetry with the *b*-system, is not anticipated in the binary black hole model. Chornock et al. (2009) instead suggest that J1536+0441 is a "double-peaked" emission-line QSO. Gaskell (2009) also suggested this interpretation, based on his evaluation of the SDSS spectrum, alone. Under this picture, the spectrum of J1536+0441 reflects instabilities in or an unusual configuration of an accretion disk around a single black hole. At the same time, Chornock et al. (2009) point out that the extreme difference in flux between the *b*-system lines and the red bumps, plus the sharp cores of the *b*-system Balmer lines, are unique among the class of double-peaked emitters.

Other interpretations are that J1536+0441 is the chance superposition of two active galactic nuclei (AGNs), or that one system is a black hole with associated AGN that has been ejected from the nucleus of the host galaxy. We showed, however, that there is only a 3×10^{-3} chance of finding any random close pair of QSOs in the entire SDSS DR7 sample searched to yield J1536+0441.[1] We also considered this hypothesis to be unsatisfactory, as there are no known examples of an isolated AGN with strong, broad Balmer lines, but no corresponding narrow lines at all. A more intriguing possibility is that the *b*-system is a black hole ejected from the nucleus of a galaxy now

* Based on observations made with the NASA/ESA *Hubble Space Telescope*, obtained at the Space Telescope Science Institute, which is operated by the Association of Universities for Research in Astronomy, Inc., under NASA contract NAS 5-26555. These observations are associated with GO/DD proposal #11993.

[1] This assumes an uncorrelated Poisson angular distribution of QSOs, which is reasonable, since the broad-line velocity difference, if interpreted as an offset in the Hubble flow, corresponds to a larger physical separation in distance than any expected correlation scale.

just hosting the *r*-system; however, the large implied ejection velocity and the light source for the absorption system are problematic.

These conclusions are challenged by Wrobel & Laor (2009), however, who obtained VLA observations of J1536+0441, showing it to comprise two sources separated by 0.″97, with 1.17 ± 0.04 and 0.27 ± 0.02 mJy flux strengths or a 4.3 flux ratio at 8.5 GHz. If these separately correspond to the two broad-line systems, then this would be a strong refutation of hypothesis that J1536+0441 is a strongly bound binary system. Prior to publication of the Wrobel & Laor (2009) observations, we requested a single orbit of *Hubble Space Telescope* (*HST*) imaging to check for multiple sources or unusual morphological features that might be diagnostic. We also obtained long-slit spectroscopy. These new observations appear to rule out the "chance superposition" or "ejected black hole" hypotheses, but leave the choice between the "double-peaked" or "binary black hole" hypotheses unresolved.

2. THE *HST* IMAGING PROGRAM

2.1. The Observations and Their Reduction

HST images of J1536+0441 were obtained on 2009 April 21 under program GO/DD 11993. The QSO was centered in the PC1 CCD of WFPC2. The duration of the program was a single orbit, sufficient to probe the morphology of the bright AGN emission and to identify bright companions. Eight short (80s) exposures were obtained in filter F675W. The bandpass of the filter includes the Hβ lines of both the *b*- and *r*-redshift systems, as well as the [O III] lines associated with the red system. The F675W images were dithered to provide 0.5×0.5 pixel subsampling to produce a Nyquist-sampled image of the system, as well as to recover the best spatial resolution available for the particular camera and filter combination. Two exposures were obtained at each dither position to permit the repair of cosmic-ray hits. The typical peak exposure in the center of the QSO subimages was $\sim 10^4 e^-$. The time remaining in the orbit after completion of the dither sequence was used to obtain two 100s spatially coincident exposures in the F439W filter to provide some level of color information, but these exposures were unfortunately much shallower, having a peak level of $\sim 1.6 \times 10^3 e^-$.

An up-sampled F675W superimage was generated from the eight individual exposures. The two exposures at each dither point were first combined, with cosmic rays identified as statistical outliers in each pair. The four summed exposures at each dither position were then combined to produce a single image with a 2× finer pixel scale (0.″0228 pixel^{-1}), using the Fourier technique of Lauer (1999). For the F675W bandpass, the *HST* optical spatial band-limit falls well short of the Nyquist scale in the up-sampled image, thus high spatial frequencies between the two scales only encodes noise and were hence eliminated from the final image by a Wiener (1949) filter. The final F439W image is just an addition of the two subexposures after cosmic ray rejection. Both images are shown in Figure 1.

2.2. The Companion Object

The F675W image of J1536+0441 shows the QSO to have a faint spatially-resolved companion. Its projected separation from the QSO is 0.″96 or 5.0 kpc in the *r*-system frame ($z = 0.388$) at 90.°1 position angle.[2] This location is well within the 0.″03 position error of the companion radio source discovered by Wrobel & Laor (2009). As we were completing this manuscript, Decarli et al. (2009) reported seeing this companion in VLT *K*-band images.

We deconvolved the F675W image using 20 iterations of the Lucy–Richardson algorithm (Lucy 1974; Richardson 1972) to gain a model independent understanding of the morphology of the companion. The point-spread function (PSF) was constructed from standard stars observed over the last several years for photometric monitoring of the F675W filter. While no F675W PSF observations were available close in time to the present observations, the attendant small uncertainties in the PSF do not affect our results. The F675W apparent magnitude of the object is 20.67 (AB) in a 0.″5 aperture. At $z = 0.388$, the F675W bandpass is very nearly centered on the SDSS *g* band. The implied absolute magnitude is −21.41, which includes the *k*-correction and a 0.13 mag correction for galactic extinction. The companion is unfortunately not visible in the F439W image; however, the zero point in this image is 2.85 mag (AB) brighter than that for the F675W superimage. Even if the companion object had a flat spectral energy distribution, the expected peak count in the F439W images would only be ∼0.5 ADU. Since the F439W filter falls to the blue of the 4000 Å break at the QSO redshift, it is likely that the true flux of the companion is even fainter. The color constraints offered by the F439W images are thus only of marginal interest.

The companion is best seen in the lower-left panel of Figure 1, in which we have attempted to subtract the QSO, which was done by scaling the reference F675W PSF to the peak flux of the QSO. The companion appears to be smooth and slightly elliptical in morphology. No tidal features are seen, nor is there any apparent connection to the QSO. However, the image is very shallow and we estimate that it would be difficult to see isolated features with surface brightnesses dimmer than ∼20.5, thus this constrains only very strong interactions.

The brightness profile is presented in Figure 2. Its form resembles that of an elliptical galaxy with a core (Lauer et al. 1995). In contrast, the profile is less well described by an exponential; if an exponential is fitted to just the outer part of the profile, the center of the profile rises well above it. An $r^{1/4}$ law fitted to the profile yields an effective radius, $R_e = 1.''23$, or 6.4 kpc. If used to estimate a total apparent luminosity, this form yields a value substantially brighter than the aperture magnitude quoted above; however, given that the brightness profile cannot be detected at $r > 0.''5$, still a small fraction of R_e, it is difficult to credit such a large extrapolation. In any case, the value of R_e, as well as the surface brightness as a function of physical radius, is consistent with that seen in early-type galaxies within a generous range of absolute luminosity about the aperture magnitude quoted above.

The most interesting aspect of the companion is its relatively strong radio emission. Wrobel & Laor (2009) derive νL_ν radio luminosities at 8.5 GHz of 5.2×10^{40} erg s^{-1} and 1.2×10^{40} erg s^{-1} for the QSO and companion, respectively. The QSO/companion radio flux ratio is thus only 4.3, as compared to the optical flux ratio of ∼30 implied by the F675W 16.99 (AB) apparent magnitude of the QSO. At the same time, Decarli et al. (2009) find the *K*-band flux ratio to be ∼5, which would imply that the companion object is very red, with the caveat raised above that our small aperture may have underestimated the total optical luminosity of the companion. The companion radio luminosity is consistent with the largest values appropriate to the most luminous "normal" early-type galaxies (Sadler et al.

[2] We assume $H_0 = 71$ km s^{-1} Mpc^{-1}, $\Omega_m = 0.27$, and a flat cosmology throughout the paper.

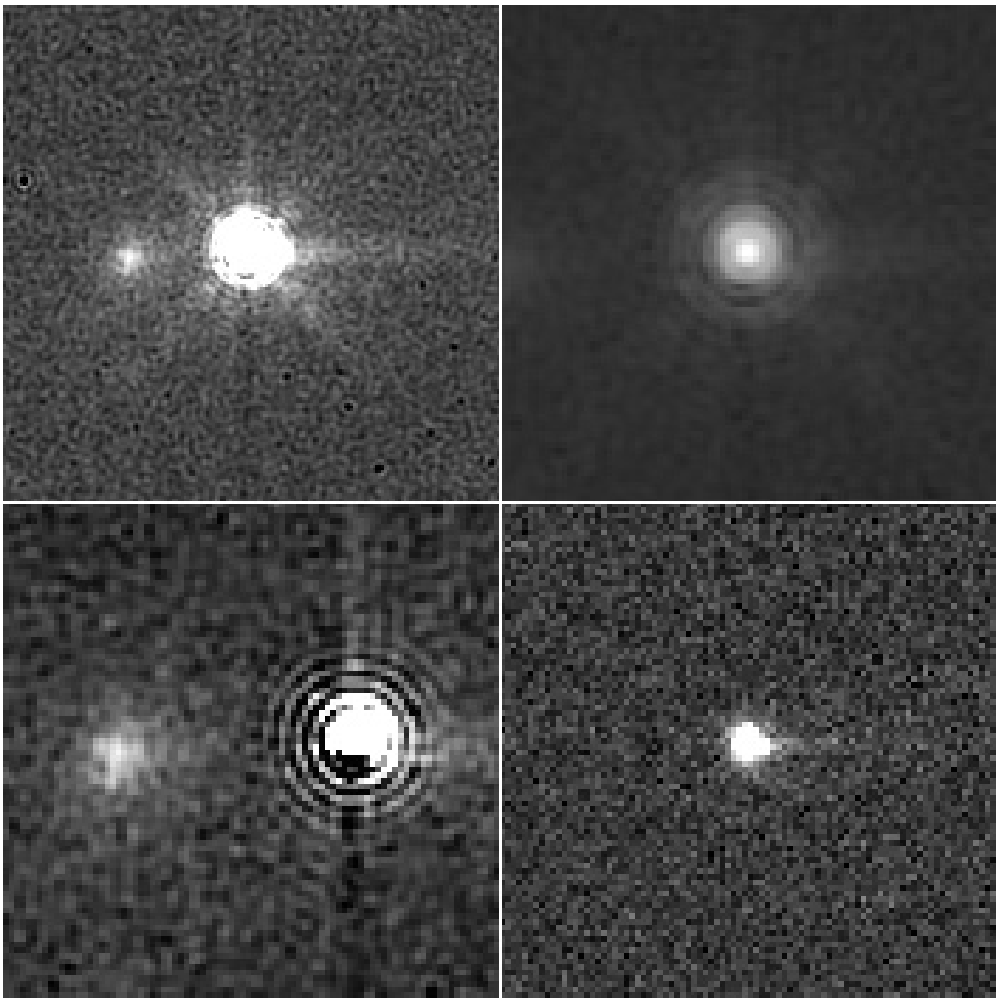

Figure 1. *HST* WFPC2/PC images of J1536+0441. North is at the top. The upper-left panel shows the central $4'' \times 4''$ of the F675W up-sampled summed image. A linear stretch has been used. The companion is left of the QSO. The upper-right panel is the central $2'' \times 2''$ of same image, but with a logarithmic stretch to show the inner structure of the QSO core. The lower-left panel shows a $2'' \times 2''$ patch of the F675W image centered between the QSO and companion after a PSF scaled to the peak of the QSO has been subtracted. The bright residuals are artifactual. The lower-right panel shows the central $4'' \times 4''$ of the F439W image. The stretch is identical to that in the upper-left panel.

1989; Wrobel & Heeschen 1991)—it is well above the typical power seen in galaxies close to the estimated absolute magnitude given above.

Despite its strong radio emission, the companion shows no obvious nuclear point-source component in the optical. This is consistent with the analysis shown in the next section that shows that the companion is not the source of the optical emission lines. Decarli et al. (2009) assert that the companion does have a point source component in contradiction of the present results. However, they present no analysis or figures to support this claim, and the spatial resolution of their *K*-band image appears to be at least an order of magnitude poorer than that of the *HST* images.

There are no other obvious sources associated with either the QSO or companion. The reference PSF and QSO core have identical morphologies within their half-light radii. In particular, we can easily rule out the presence of an additional point source having a flux exceeding 10% of the QSO centered at any distance greater than $0\farcs1$ from the QSO. At slightly larger radii, the residuals of the PSF subtraction show a largely dipole pattern, with excess light seen to the northwest of the QSO in Figure 1. While, as noted earlier, there is very little recent stellar imaging available in the F675W filter, examination of standard stars observed in the F555W or F547M filters a few months prior to execution of the present program show this pattern to be common; it is consistent with a small amount of comatic aberration. We thus conclude that the residual pattern is artifactual. The residuals also make it difficult to set any constraints on the properties of the QSO host galaxy. On the assumption that the QSO subtraction residuals are largely due to a host galaxy, rather than a miss-match between the PSF and QSO core, the implied host luminosity is less luminous than $M_g \sim -22$.

3. THE SPECTROSCOPY

3.1. Observations and Their Reduction

Spectra of J1536+041 were obtained on the night of April 22 (UT) with the RC spectrograph on the Mayall 4 m telescope at Kitt Peak. The BL 420 grating provides a 1.5 Å pixel^{-1} dispersion; in combination with a $1\farcs5$ wide slit, the resulting resolution is between 3.0 Å and 3.6 Å over the wavelength ranges covered. Two grating tilts were used, a blue setting to cover the region from 5000 Å to 7600 Å and a red setting to cover the region from 7000 Å to 9500 Å. The slit was $49''$ long and was oriented east–west to capture the companion seen

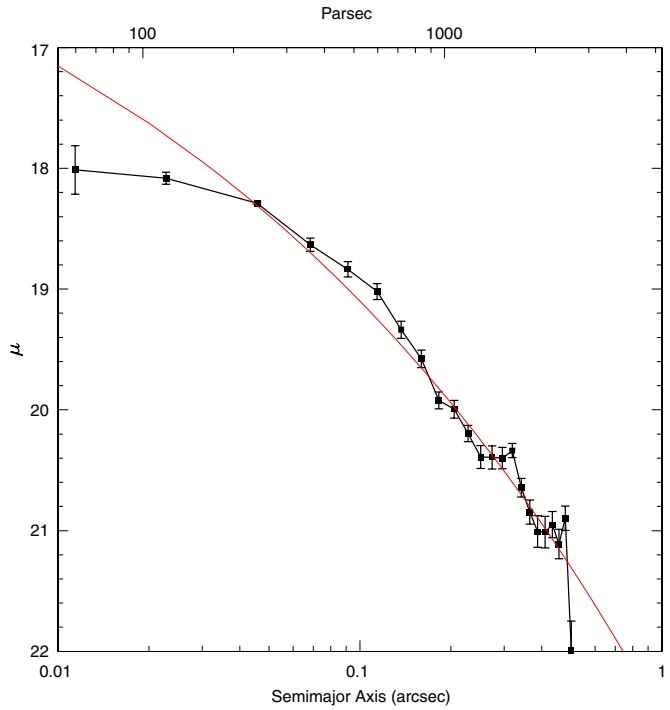

Figure 2. Deconvolved brightness profile of the companion object is plotted (black). The error bars are based on scatter observed around the individual isophotes; and uncertainty in the deconvolution for the central point. The surface brightness is as observed—no extinction or cosmological corrections have been applied. The bandpass at the QSO redshift is essentially SDSS *g* band. The red line shows an $r^{1/4}$ law fitted to the profile for $r > 0\farcs04$.

(A color version of this figure is available in the online journal.)

in the *HST* images. The spatial pixel scale is $0\farcs69$ pixel^{-1}. Five exposures were obtained with the blue setting, and four exposures were obtained with the red setting. All exposures were 900 s. The seeing was poor during the period of the observations; a Gaussian fit to the object flux along the slit gives about $1\farcs7$ FWHM. In addition to the exposures on the object itself, helium–neon–argon comparison spectra were obtained at the object position and flux standard stars were observed with the same setup.

The spectra were reduced by removal of bias, division by a flat field, subtraction of the sky spectrum, and extraction of a one-dimensional spectrum from a region of the frame extending about 2″ on either side of the spatial peak. The flux standards were used for both removal of atmospheric absorption features and for flux calibration. Positions of several dozen lines in the helium–neon–argon spectra were fit to low-order polynomials, resulting in wavelength calibrations accurate to 0.08 Å rms for the bluer setting and 0.09 Å rms for the redder setting. The individual spectra of each wavelength region were then combined, though some of the measurements described below were made from the individual exposures in order to estimate the uncertainty from the scatter. The final combined spectrum is shown in Figure 3.

The new spectrum is quite similar to the SDSS spectrum. In addition to the complicated structure of the Balmer lines, discussed in the next section, the same narrow lines are seen, including [O II] λ3727, [O III] λ4363, λ4959, and λ5007, and [Ne III] λ3869 and λ3968. In addition, the [N II] λ6584 line is now visible on the red side of the *r*-system Hα line. The narrow absorption lines of Na I D and Ca II H are also seen.

Our new spectrum has somewhat higher signal-to-noise than does the SDSS spectrum in the region between 5500 Å and

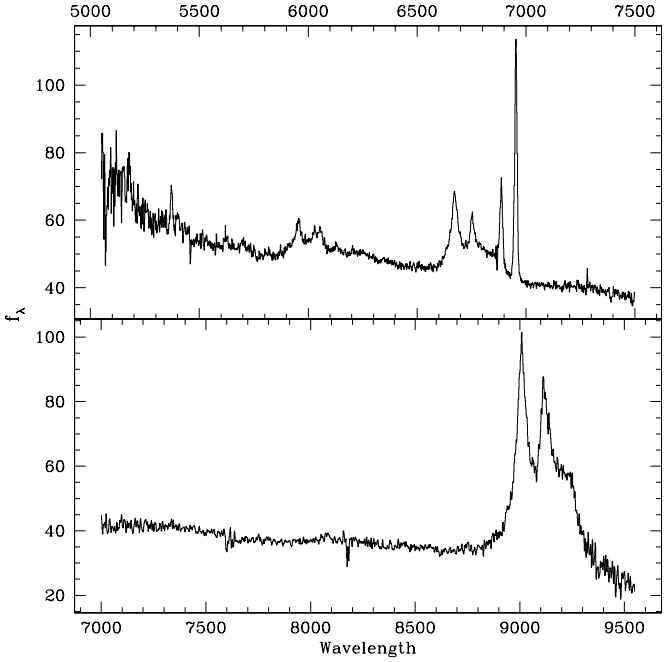

Figure 3. New spectrum of J1536+0441 obtained with the RC Spectrograph on the Mayall Telescope. The observed wavelength scale for the bluer region (top panel) is given on the top of the figure; that for the redder region (bottom panel) is given on the bottom. Fluxes are in units of 10^{-17} erg cm^{-2} s^{-1} Å^{-1}.

6500 Å and the Hδ lines for the *b*- and *r*-systems are visible. In addition, the Fe II emission between Hγ and Hβ is easier to distinguish than in the SDSS spectrum. We attempted to determine whether it comes predominantly from the *b*- or *r*-system by cross-correlation with the corresponding region from the Fe II template developed by Boroson & Green (1992) from the spectrum of I Zwicky 1. This cross-correlation shows that the optical Fe II is primarily associated with the *b*-system velocity, though the signal-to-noise is not sufficient to rule out a contribution from the *r*-system as well.

3.2. The Balmer Line Profiles

The new data clearly show that the combined profiles of the Balmer lines extend as far to the red from the narrow-line redshift as they do to the blue, as pointed out by Chornock et al. (2009). This is particularly clear in the case of Hα, which appears to extend to the red from the *r*-system at a constant level, and then drops off at about 9260 Å, which corresponds to about 4700 km s^{-1} in the rest frame of the *r*-system. This makes the bottom part of the profile approximately symmetric on the red and blue sides.

It is unclear how to measure the strengths, widths, and shapes of the various components that make up this profile. Relative to the continuum level, the *b*-system peak of Hα is 1.24 times the height of the *r*-system peak. Relative to the level of the flat part of the red shoulder, that factor becomes 1.45. We measure the equivalent width of the entire Hα complex as 348 Å, with 247 Å of that total in the broad base, defined with a flat top at the level of the red shoulder, and with 44 Å and 57 Å as the contributions of the *r*-system and *b*-system peaks, respectively.

3.3. Profile Changes Between the Two Epochs

The most compelling confirmation that this system is a supermassive black hole binary would be the measurement

of changes in the radial velocities of the two peaks consistent with orbital motion. In Boroson & Lauer (2009), we estimated the separation of the two black holes to be 0.1 pc with a ~ 100 year orbital period, based solely on the implied radial velocity difference, an estimate of the two black hole masses, and the assumption of mean values for the orbital phase and inclination. These numbers predict a measurable change in velocity separation of the two peaks in as little as a year. Our new spectrum was obtained 1.04 years after the SDSS 2008 April observation, which corresponds to 0.75 years in the rest frame of the object.

Visual inspection of the new spectra, as well as the report of Chornock et al. (2009), shows that changes in the separation of the peaks of the Balmer lines are small or absent. Until and unless these changes become significant, improved constraints on the orbital parameters are based instead on the size of the errors bounding a null measurement.

Given the complex structure of the Balmer line profiles, measurement of accurate velocity requires that the spectra at all epochs and from all sources be treated consistently. In particular, a consequence of the composite nature of the profile is the possibility that the Hα and Hβ lines in each system may have different behavior. We note specifically that there is a well-established trend of decreasing Balmer decrement with velocity away from the line center in Seyfert galaxies and QSOs (Shuder 1982; Crenshaw 1986). That is, the wings of the Hα line fall off more quickly than those of the Hβ line. This effect appears to be present in the *r*-system Balmer lines, and it results in a larger gradient under the *b*-system Hα line than under the Hβ line, leading to the perception that the splitting between the two systems is less in the Hα line than in the Hβ line. However, if one overplots the Hβ and Hα regions with a relative shift equal to the ratio of the rest wavelengths of the lines, it can be seen that the peaks of the two *b*-system lines are in excellent velocity agreement.

In order to minimize such effects, we have remeasured the SDSS spectrum and our new spectrum in the same way, emphasizing the peaks of the lines, which should be less sensitive to underlying gradients. We find that relative to the [O III] lines, the *r*-system Hβ peak has a velocity of 61 ± 15 km s^{-1}, while the *b*-system Hβ peak has a velocity of -3484 ± 35 km s^{-1}. The uncertainties quoted are the mean error as derived from the scatter in the five independent observations. The corresponding velocities from the SDSS spectrum are 31 km s^{-1} and -3512 km s^{-1} for the *r*- and *b*-system Hβ peaks, respectively. Thus, the Hβ splitting has changed from -3543 to -3545 ± 38 km s^{-1}. Similarly, we measure the Hα splitting as -3514 km s^{-1} in the SDSS spectrum and -3497 ± 40 km s^{-1} in our new spectrum. A final caveat is that there is some Balmer emission associated with the narrow lines though it is difficult to isolate, and this may influence the measured velocities of the *r*-system broad lines.

In summary, we see no shift in the positions of the Balmer line peaks over this period, with a two sigma limit of about 80 km s^{-1}.

Lastly, we investigate changes in the strengths of the peaks using the Hβ line because it is well covered in both spectra. In addition, the [O III] lines should not change and so they provide some check on our result. After rebinning the new and SDSS spectra to the same resolution, we find that changes in the strengths of the two peaks relative to the continuum and to each other can be limited to less than 3% over the period between the two observations.

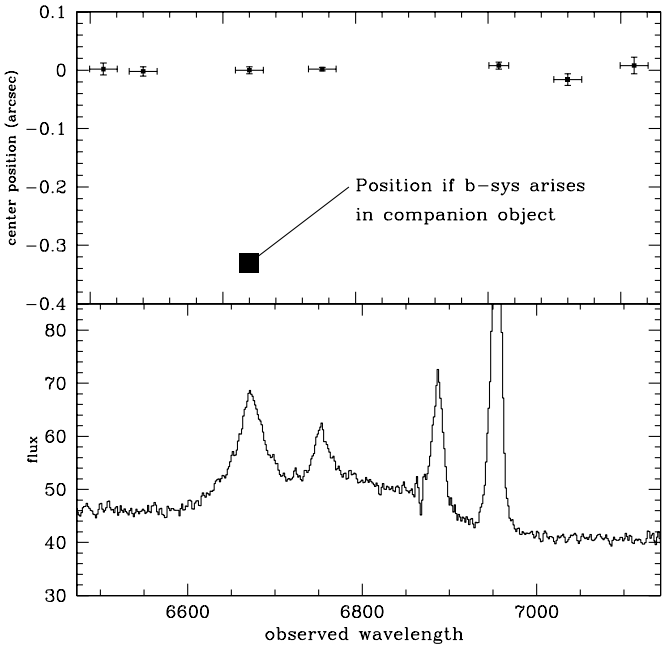

Figure 4. Top panel shows the spatial location along the slit of the flux-weighted centroid of the spectrum in bands shown by the horizontal error bars. The vertical error bars show the standard deviation in the measured positions from five independent exposures. The lower panel shows the spectral flux through this region. The bands have been chosen to represent (from left to right) two continuum regions, the *b*-system Hβ line, the *r*-system Hβ line, the [O III] λ5007 line, and two more continuum regions. The square indicates where the point representing the *b*-system Hβ line would fall if it arose in the companion object.

3.4. Spatial Location of Spectral Features

Wrobel & Laor (2009) speculate that one of the two strong peaks in the Balmer line profiles may arise in the companion source seen in the radio. Since our slit was aligned east–west, and the separation between the two objects is approximately 1 arcsec, this would result in an easily visible offset in the spatial location of the spectrum at the position of any feature arising in the companion. To test this idea, we fitted the intensity of the spectrum along the slit as a function of wavelength at positions corresponding to the *b*- and *r*-system Hβ lines, the two [O III] lines, and four continuum points spanning this region. The centers of the best-fit Gaussians are shown in Figure 4. We have removed a linear tilt in the spectrum, due to a slit misalignment of the dispersion with respect to the CCD rows. The horizontal error bars show the range of the columns of the frame averaged. The vertical error bars show the standard deviations in the five measurements made from the five independent exposures. The corresponding spectrum is shown in the lower panel of Figure 4.

An estimate of the expected shift if the *b*-system arose in the companion object can be obtained by noting that the equivalent width of the *b*-system Hβ line is approximately 15 Å in the "composite" spectrum and that the width of the region averaged together is approximately 30 Å. Since the ratio of flux in the companion object is only about 1/30 of that in the primary object within this spectral region, not much of the continuum can arise in the companion. This results in a relative flux within this 30 Å window of about 2 to 1 in favor of the brighter object, producing a position that would be offset by 1/3 of the 1 arcsec separation. This is obviously incompatible with the measured

positions, leading us to conclude that all of the spectral features arise in the primary object.

4. WHAT J1536+0441 COULD BE AND WHAT IT ISN'T

The analysis of the new *HST* images and KPNO spectra of J1536+0441 appears to rule out some hypotheses on its physical configuration, while leaving the door open to others that are likely to require additional observations for further evaluation. We close by summarizing what we conclude is the current status of the various explanations for the unusual properties of J1536+0441.

4.1. Chance Superposition of Objects

The discovery of Wrobel & Laor (2009) that J1536+0441 is a well-resolved binary radio source appears to argue for the conclusion that it is simply the line of site superposition of two AGNs, a conclusion also advocated by Decarli et al. (2009). Boroson & Lauer (2009) did not favor this hypothesis, as the probability of a superposition was low (3×10^{-3}), and required one of the AGNs to have unique behavior in exhibiting broad lines without any corresponding narrow lines. In advance of the *HST* observations, we might have expected to see the QSO resolved into two point sources, corresponding to two physically separate AGNs. Alternatively, we might have seen an optical jet emerging from the QSO. The optical counterpart to the less-luminous radio source, however, appears to be a normal galaxy with no evidence for an optically visible AGN, based both on the *HST* imagery, and analysis of the angular centroids of the emission lines in the long-slit spectroscopy. Superficially, it thus appears that this object is merely an "innocent bystander" to J1536+0441, although its large radio luminosity remains unexplained in this scenario. One possibility, however, is that it at least is the source of the absorption lines seen in its spectrum. The "*a*-system" has a projected velocity of 240 km s^{-1} less than the *r*-system, compatible with galaxy and the QSO forming a binary system.

Wrobel & Laor (2009) derived a considerably higher a priori probability of superposition than our estimate quoted above. Using the Hennawi et al. (2006) QSO–QSO correlation function, they derived a probability of about unity for the occurrence of a 5 kpc separation pair within the size the original sample studied by Boroson & Lauer (2009). We note, however, that Hennawi et al. (2006) limited their sample of QSO pairs to those with $\Delta V < 2000$ km s^{-1}, on the assumption that larger velocity separations would not be expected in systems that are truly physically associated. Croom et al. (2005), for example, show no significant correlation between QSOs with velocity differences as large as that in J1536+0441. A possible exception to this would be for two QSOs both bound in the potential of an extremely rich cluster. Heckman et al. (2009), for example, hypothesize that the two emission line systems separated by 2650 km s^{-1}, in the QSO SDSSJ092712.65+294344.0 is a system analogous to the $\sim$3000 km s^{-1} difference between the two emission line systems seen in NGC 1275 (Minkowski 1957), the first-ranked galaxy of the Perseus galaxy cluster. The probability of this occurrence for J1536+0441 should be encoded in the Croom et al. (2005) function, however.

The limit on spatial coincidence from the new *HST* images, however, is now at least 2 orders of magnitude more stringent than that assumed in Boroson & Lauer (2009) or Wrobel & Laor (2009). This argument continues to disfavor the idea that there are two separate host galaxies.

4.2. Ejected Black Hole

If one assumes that the *r*-system, which includes the narrow-line system, represents the rest velocity of the host galaxy, then in advance of the present observations, one might have hypothesized that the *b*-system represented a black hole ejected from the nucleus. There are two ways to achieve this result. Under the first mechanism, as two black holes merge, an asymmetric jet of gravitational radiation can be emitted, propelling the merged black hole out of the nucleus. In the second mechanism an infalling black hole interacts with preexisting binary black hole and is ejected in an exchange of orbital energy that binds the binary tighter and expels the third black hole.

In the case of ejection of a merged black hole, the 3500 km s^{-1} velocity of the *b*-system is at the edge of plausible ejection velocities that have been demonstrated in numerical experiments (Campanelli et al. 2007; González et al. 2007). Such high velocities depend on very specific mass ratios, spins, and orbital parameters of the merging black holes, and appear to be extremely unlikely. Schnittman & Buonanno (2007) show that the probability of ejection velocities in excess of $\sim$3000 km s^{-1} may occur in $\ll 0.1\%$ of all black hole mergers. Regardless, while this might explain the QSO as two separate objects, one of which has been ejected, the spatial centroid of the Hβ lines show that neither of these objects resides in the companion galaxy.

Ejection as the result of the interaction of an infalling black hole with a pre-existing binary black hole may also produce relative velocities in excess of $\sim$3000 km s^{-1} under rare conditions. The distribution of ejection velocities presented by Hoffman & Loeb (2007) shows that these may occur in a few percent of the interactions, thus apparently making this mechanism much more likely to produce a high-velocity ejection than the merger case. This mechanism allows for the existence of two AGNs after the ejection, and thus might have explained J1536+0441 had the present observations revealed two distinct sources of optical emission. As with the merger case, however, it cannot explain the spectrum of J1536+0441 as a single source.

On observational grounds, we did not favor this hypothesis in Boroson & Lauer (2009), as the high velocity of the *b*-system, but the unresolved nature of the point source implied either that the system was being observed close to the epoch of its creation, or that the ejected black hole was essentially traveling along the line of sight. It was also difficult to understand the geometry under which the *b*-system AGNs could serve as a continuum source against which the *a*-system absorption lines are seen.

If the *a*-system is attributed to the companion galaxy, then the geometry under which the *a*-system is seen against the QSO may be more plausible. The tighter restrictions placed on the ejection geometry by the *HST* imagery makes this even less attractive, however.

We also note the superficial similarity of J1536+0441 to the object HE 0450−2958, which has been proposed as a "naked" QSO (Magain et al. 2005; Kim et al. 2007), possibly ejected from a disturbed galaxy about 1.″5 away (Letawe et al. 2009). Although the projected separation between the QSO and the putative host, 6.5 kpc, is similar to the separation between J1536+0441 and the companion object, there are two critical differences. First, the upper limit we have derived for an underlying host galaxy at the position of the J1536+0441 nucleus, $M_g \sim -22$, is still bright enough that no alternative host is required. Second, this explanation does not account for the unique spectrum of J 1536+0441; the QSO in the GE 0450−2958 system has a normal spectrum.

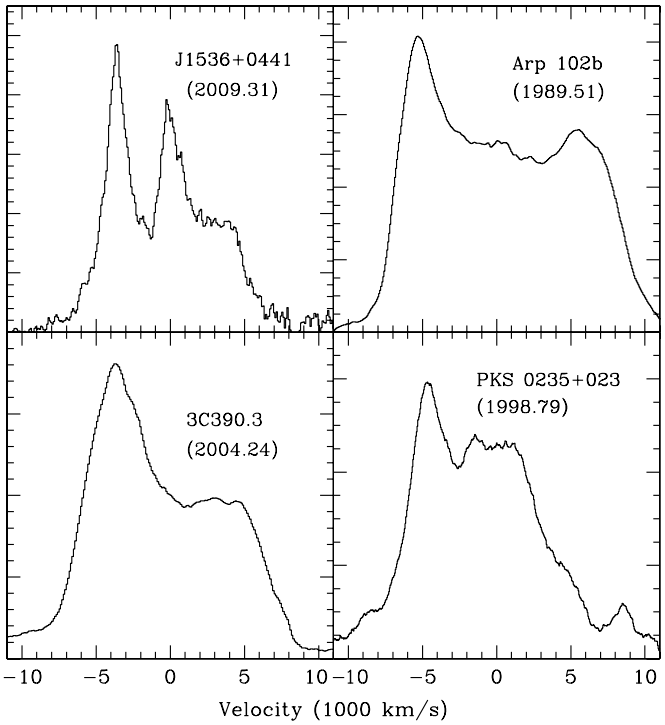

Figure 5. Comparison of the Hα profile of J1536+0441 with three objects classified as double-peaked line emitters potentially analogous to J1536+0441 from the study by Gezari et al. (2007). Each object is identified and the epoch of the observation is given. The epochs of the comparison objects were chosen as those with profiles that most closely matched J1536+0441 in terms of the ratio of the strengths of the two peaks. The narrow lines have been removed from the comparison objects, and the continuum has been subtracted from all the objects. The narrow lines in J1536+0441 are insignificant.

4.3. Double-peaked Emitter

The most attractive explanation for J1536+0441 may indeed be that it is a "double-peaked" emission line QSOs. The red bumps in the broad lines discovered by Chornock et al. (2009), and confirmed here, certainly resemble some of the broad and diffuse emission seen in these objects. The double-peaked class is further already known and admits a variety of unusual broad-line profiles. At the same time, there are striking differences between the Balmer line profiles in J1536+0441 and those of the double-peaked objects generally.

The prototypical profile of the double-peaked objects has two rounded peaks of roughly equal strength joined by a flat or depressed central plateau. This form can be well fitted by simple relativistic accretion disk models (Chen et al. 1989; Strateva et al. 2003; Gezari et al. 2007). These objects occasionally show substantial departures from this form, in which relatively sharp, transient peaks are seen. Michael Eracleous at our request selected three cases of such profiles from the compilation of Gezari et al. (2007); these are shown together with the Hα profile of J1536+0441 in Figure 5. The narrow lines, Hα, [N II], [S II], and [O I], have been removed from the double-peaked lines. In the case of J1536+0441, the narrow lines are very weak, the [N II] λ6584 line is just barely visible on the red wing of the *r*-system Hα line, and the other lines are not detectable at all.

Although we admit that the detailed accretion disk structure that leads to these profiles is not well understood, we observe several notable differences between J1536+0441 and these objects. (1) J1536+0441 has a strong, central, broad peak, which is not seen in any of the double-peaked emitters. (2) The blue peak in J1536+0441 is very strong and very narrow at its top, surpassing, though perhaps by only a small amount, these characteristics in any of the other objects. (3) The strong, sharp peaks in the double-peaked emitters are transient. In all three of these objects, the blue peak showed large changes in its intensity over a few months to less than a year. J1536+0441, on the other hand, has shown a constant profile for almost a year now.

It is worth noting that the double-peaked emitters themselves were initially advanced as binary-black hole candidates. It is only the failure of the lines to vary in velocity over long time spans that has led to alternative interpretations of this class. Nor is there a clear theory on how the asymmetries accretion disks in these systems are generated or maintained. If J1536+0441 is a member of this class, then it may well motivate an improved picture of how disk instabilities arise and evolve.

4.4. A Binary Black Hole

The new observations presented here and those of Chornock et al. (2009) do not advance the hypothesis that J1536+0441 hosts a binary black hole, except by perhaps eliminating the superposition and ejected black hole hypotheses. The lack of any observed velocity shift in the *b*-system or *r*-system over the span since the original SDSS spectrum was obtained provides additional constraints on the orbital parameters. The prediction that velocity shifts could be seen within a year was based on the presumption of an average viewing geometry and orbital phase for the binary system. If, however, the velocity difference between the *b*- and *r*-systems represents a substantial portion of the orbital velocity, then the orbital radius of the system is larger, and the period longer than the estimates given in Boroson & Lauer (2009). The geometry also requires longer intervals to see velocity changes if the system is close to quadrature.

The derived orbital parameters also depend on the total mass of the binary system, which was estimated by Boroson & Lauer (2009) from the widths of the Hβ lines and the continuum luminosity. The assumption that the two black holes were emitting at the same fraction of their Eddington luminosities resulted in estimates of $10^{7.3}$ and $10^{8.9} M_\odot$ for the *b*- and *r*-systems, respectively. The discovery of the extension of the Balmer line profiles to the red allow us to revisit this calculation. Replacing the former value of 6000 km s^{-1} with a new measured value of 10,600 km s^{-1} for the *r*-system FWHM results in the increase of that black hole to $10^{9.4} M_\odot$. Two other methods can be used to estimate the black hole masses. The width of the [O III] λ5007 line can be used as a surrogate for the stellar velocity dispersion (Salviander et al. 2007), yielding a mass of $10^{8.4} M_\odot$. Also, one can get a handle on the mass by adopting an average value of $L/L_{\rm Edd}$, 0.14, for QSOs with the redshift and luminosity of this object (Shen et al. 2008), which results in a mass of $10^{8.7} M_\odot$.

We explored the new constraints from our spectroscopy in two different ways. First, we calculated the expected velocity change for all possible values of the inclination and initial phase over the time period between the SDSS spectrum and our new spectral observation. We assume that the orbit is circular. Figure 6 shows the allowed and excluded regions, given our 2σ limit on the velocity change of 80 km s^{-1} for two different values for the total system mass, 1×10^9 and $3 \times 10^9 M_\odot$. This confirms the qualitative statement above—the allowed orbits are those in which the inclination is closer to line of sight and the initial phase is closer to maximum elongation. These are the cases for which the observed velocity difference between the two

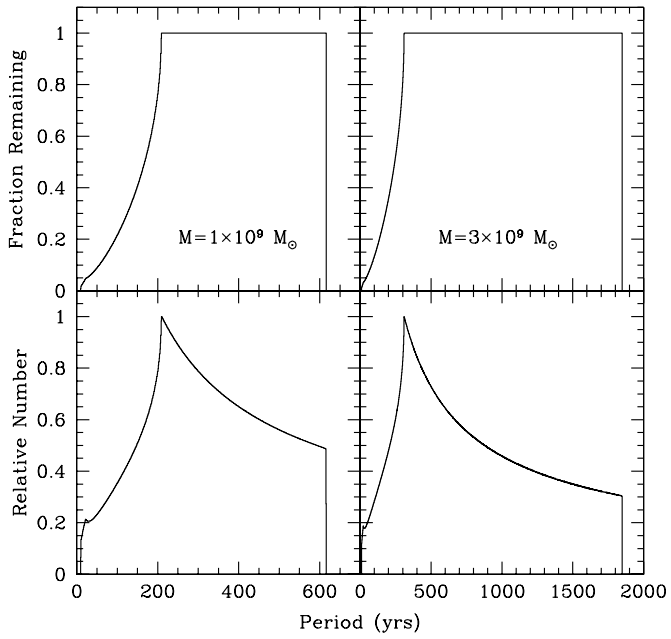

Figure 6. Orbital parameter space for binary black hole model, showing allowed range of inclination and phase at $t = 0$ (2008.27). Excluded regions come from 2σ limit of 80 km s^{-1} between original SDSS observation and KPNO observation reported here. Shown are regions excluded for a total system mass of 1^9 $M_\odot$ (yellow) and 3×10^9 $M_\odot$ (blue shading).

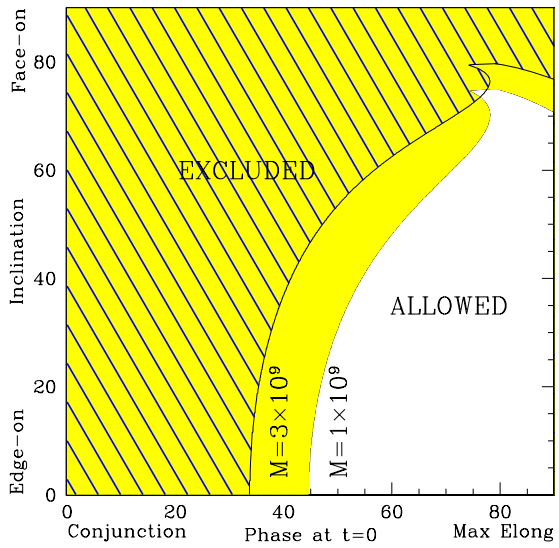

Figure 7. Fraction of binary orbits as a function of period that are permitted by the new spectroscopic observation. The right and left panels show calculations for a total system mass of 1×10^9 and 3×10^9 solar masses, respectively. The top panels show the fraction of original possible orbits remaining; the bottom panels show the distribution of those remaining orbits over period. The median remaining period is 319 years for the smaller total mass and 743 years for the larger total mass.

(A color version of this figure is available in the online journal.)

systems represents a larger fraction of the true space velocity difference.

While this exercise demonstrates the values of initial phase and inclination that are still permitted, it does not show the fractional reduction in allowed orbits, nor does it show the range of allowed periods. These are shown in Figure 7 for the two system masses we investigated. The top panels show the fraction of original orbits that remain possible as a function of the orbital period. None of the periods longer than 200 years has been ruled out. The remaining possible orbits account for 43% and 56% of the original orbits for the smaller and larger system masses. The lower panels show the relative number of possible orbits remaining as a function of period. The median values for the period of the remaining orbits are 319 and 743 years for the smaller and larger system masses.

As we pointed out, the differences between the observed Balmer line profiles and those seen in double-peaked emitters, we must also note that the newly discovered extension of the profiles to the red is problematic for the binary explanation. Rather than a model in which two separate massive objects are orbiting a center of mass located between them, this profile suggests that the smaller object might be embedded in (or passing through) the disk surrounding the larger one. The extension to the red could result from waves or disturbances in the disk as a result of this interaction.

It is clear that the ultimate confirmation or rejection of the possibility that the blue emission-line peak represents an object in orbit around a central object will come from a number of years of spectroscopic monitoring.

We thank Matt Mountain for the grant of STScI Director's Discretion time under which the *HST* observations were obtained. We thank the STScI support staff for prompt and expert assistance in the preparation of the observing program. We thank Buell Jannuzi for the availability of the KPNO 4 m time. We thank Matthew Lallo for discussions on the properties of the WFPC2/PC1 PSFs. We thank Michael Eracleous for useful conversations on the properties of "double-peaked" emitters, and for identifying potential analogues to J1536+0441. We thank Suvi Gezari for providing us with the Hα spectra of these analogues. The National Optical Astronomy Observatory is operated by AURA, Inc., under cooperative agreement with the National Science Foundation.

REFERENCES

Boroson, T. A., & Green, R. F. 1992, ApJS, 80, 109
Boroson, T. A., & Lauer, T. R. 2009, Nature, 458, 53
Campanelli, M., Lousto, C., Zlochower, Y., & Merritt, D. 2007, ApJ, 659, L5
Chen, K., Halpern, J. P., & Filippenko, A. V. 1989, ApJ, 339, 742
Chornock, R., et al. 2009, ATel, 1955, 1
Crenshaw, D. M. 1986, ApJS, 62, 821
Croom, S. M., et al. 2005, MNRAS, 356, 415
Decarli, R., Treves, A., Falomo, R., Dotti, M., Colpi, M., & Kotilainen, J. K. 2009, ATel, 2061, 1
Gaskell, C. M. 2009, arXiv:0903.4447
Gezari, S., Halpern, J. P., & Eracleous, M. 2007, ApJS, 169, 167
González, J. A., Hannam, M., Sperhake, U., Brügmann, B., & Husa, S. 2007, Phys. Rev. Lett., 98, 231101
Heckman, T. M., Krolik, J. H., Moran, S. M., Schnittman, J., & Gezari, S. 2009, ApJ, 695, 363
Hennawi, J. F., et al. 2006, AJ, 131, 1
Hoffman, L., & Loeb, A. 2007, MNRAS, 377, 957
Kim, M., Ho, L., Peng, C., & Im, M. 2007, ApJ, 658, 107
Letawe, G., Magain, P., Chantry, V., & Letawe, Y. 2009, MNRAS, 396, 78
Lauer, T. R. 1999, PASP, 111, 227
Lauer, T. R., et al. 1995, AJ, 110, 2622
Lucy, L. B. 1974, AJ, 79, 745
Magain, P., et al. 2005, Nature, 437, 381
Minkowski, R. 1957, Radio Astron., 4, 107
Richardson, W. H. 1972, J. Opt. Soc. A, 62, 52
Sadler, E. M., Jenkins, C. R., & Kotanyi, C. G. 1989, MNRAS, 240, 591
Salviander, S., Shields, G. A., Gebhardt, K., & Bonner, E. W. 2007, ApJ, 662, 131

Schnittman, J. D., & Buonanno, A. 2007, ApJ, 662, L63
Shen, Y., Greene, J. E., Strauss, M. A., Richards, G. T., & Schneider, D. P. 2008, ApJ, 680, 169
Shuder, J. M. 1982, ApJ, 259, 48
Strateva, I. V., et al. 2003, AJ, 126, 1720
Volonteri, M., Haardt, F., & Madau, P. 2003, ApJ, 582, 559
Wiener, N. 1949, Extrapolation, Interpolation, and Smoothing of Stationary Time Series (New York: Wiley)
Wrobel, J. M., & Heeschen, D. S. 1991, AJ, 101, 148
Wrobel, J. M., & Laor, A. 2009, ApJ, 699, 22